Present Climate and Future Changes in the Annual Cycle of TC Activity in the WNP Investigated by HighResMIP GCMs

KUAN-CHIEH CHEN,[a] CHI-CHERNG HONG,[a] CHIH-HUA TSOU,[b] AND DING-RONG WU[c]

[a] *Department of Earth and Life Sciences, University of Taipei, Taipei, Taiwan*
[b] *Department of Earth Sciences, National Taiwan Normal University, Taipei, Taiwan*
[c] *Department of Atmospheric Sciences, National Taiwan University, Taipei, Taiwan*

(Manuscript received 18 January 2024, in final form 6 June 2024, accepted 20 June 2024)

ABSTRACT: Atmospheric general circulation models (AGCMs) and coupled general circulation models (CGCMs) in the High Resolution Model Intercomparison Project (HighResMIP) were evaluated on their ability to simulate tropical cyclone (TC) activity in the western North Pacific (WNP) over its annual cycle. Specifically, we examined these models' ability to simulate the south–north migration of the mean TC genesis location. The results revealed that both types of models realistically captured TC numbers and the south–north migration of TC genesis locations associated with the meridional migration of the WNP subtropical high ridge in response to the annual cycle. However, TC numbers decreased less rapidly in the AGCMs than in both the CGCMs and observed data during the monsoon retreat period (after September). This bias was probably attributed to a low-tropospheric cyclonic anomaly over the Philippine Sea in response to La Niña–like sea surface temperature (SST) differences between the AGCMs and the CGCMs. Because of these differences, the TC genesis frequency in the AGCMs over the Philippine Sea was overestimated. The cyclonic anomaly occurred when the northeasterly trade wind arose and was maintained through wind–evaporation–SST feedback. In future climate (2021–50), the main changes occurred during the monsoon retreat period. A more rapid decrease in TC numbers shown in AGCMs was likely attributed to the decrease (increase) of low-level vorticity (vertical wind shear) modulated by enhanced WNP subtropical high and subsidence anomalies. Conversely, a cyclonic circulation and ascending anomalies projected by CGCMs were identified off-equator, which favored TC genesis location shifting northward.

SIGNIFICANCE STATEMENT: Model performance and future changes in the annual cycle of tropical cyclone (TC) activity in the western North Pacific are investigated. We found that high-resolution uncoupled and coupled models realistically captured the TC numbers and meridional migration of TC genesis locations associated with the meridional migration of subtropical high ridge. However, TC numbers decreased more gradually in the uncoupled models than in the coupled models after September. This lower skill may stem from differences between the uncoupled and coupled models in simulating a cyclonic anomaly over the Philippine Sea in response to the La Niña–like sea surface temperature difference. In future climate (2021–50), TC numbers are significantly projected to decrease more rapidly during the monsoon retreat period in uncoupled models.

KEYWORDS: Atmosphere-ocean interaction; Atmospheric circulation; Hurricanes/typhoons; Climate change; General circulation models; Seasonal cycle

1. Introduction

The western North Pacific (WNP) is the region in the tropics where most tropical cyclones (TCs) originate from, and the TC activity in that area has a clear annual cycle (Lander 1994; Chia and Ropelewski 2002; Wang and Chan 2002; Gilford et al. 2017; Sobel et al. 2021). The analysis of TC genesis locations in response to the annual cycle reveals a clear pattern of south–north migration. The TC frequency increases significantly, and the genesis location extends northeastward starting from June, reaching the highest and northernmost location in August and September, then rapidly decreasing and returning southward in October (Chia and Ropelewski 2002; Wang and Chan 2002). This meridional migration of TC formation indirectly influences the landfall frequency of TCs over East Asia (Harr and Elsberry 1991; Kim et al. 2005). Thus, an understanding of model's ability to simulate the seasonal cycle of TC activity will be beneficial for the countries in East Asia for disaster preparedness, response, and mitigation strategies.

The south–north migration of the TC genesis location is primarily associated with the meridional migration of monsoon trough in response to the annual cycle (Ritchie and Holland 1999). The northernmost location of monsoon trough is mainly bounded by the WNP subtropical high (WNPSH), which also experiences seasonal meridional migration (Chen et al. 2017; Li et al. 2024). The WNPSH moves northward in June and reaches its northernmost location in August and September and then begins to migrate southward in October (Chen et al. 2017). The meridional movement of TC formation is substantially affected by the seasonal variation of the WNPSH, which is usually accompanied by low-level anticyclonic vorticity, low humidity, and downward motion, providing unfavorable conditions for TC development (Liu and Chan 2013;

Corresponding author: Chi-Cherng Hong, cchong@utaipei.edu.tw; hong0202@gmail.com

DOI: 10.1175/JCLI-D-24-0048.1

Wang and Wang 2019). Accordingly, the skill in simulating WNPSH is crucial to reproduce the south–north migration of the TC genesis location. Previous studies reported that air–sea coupled general circulation models (CGCMs) from phase 5 of the Coupled Model Intercomparison Project (CMIP) (CMIP5) improved the summer monsoon and WNPSH simulations at the cost of negative sea surface temperature (SST) bias in the WNP compared to those in uncoupled GCMs (Song and Zhou 2014; Yang et al. 2019). That is the cold bias in the WNP has a compensation effect on improving the WNPSH. This colder SST bias in the WNP was also identified in CMIP6 simulations (Zhang et al. 2023). How the cold bias affects the WNPSH simulation and the south–north migration of TC activity in response to the annual cycle deserves attention. However, this topic so far has been less investigated.

The ability of models to simulate the south–north movement of the TC genesis location is closely related to the ability of models to simulate the intensity and landfall frequency of TCs. Numerous studies have employed GCMs to simulate and predict the annual cycle of TC activity (Camargo 2013; Roberts et al. 2015; Dwyer et al. 2015; Roberts et al. 2020a; Sharmila et al. 2020; Tang et al. 2022). Studies have reported that models with higher horizontal resolution better simulate TC activity and TC number over the annual cycle (Manganello et al. 2012; Roberts et al. 2015, 2020a; Tang et al. 2022; Chen et al. 2023). The High Resolution Atmospheric Model (HiRAM) and downscaling models from the CMIP3 and CMIP5 are able to capture the annual cycle of TC numbers in the WNP (Dwyer et al. 2015; Tsou et al. 2016). However, high-resolution downscaling models from CMIP3 and CMIP5 have been shown to underestimate TC numbers during the peak TC season (Dwyer et al. 2015). Tang et al. (2022) found that both uncoupled and coupled simulations in CMIP6 High Resolution Model Intercomparison Project (HighResMIP) realistically captured the annual cycle of TC genesis. Their study also showed that coupled runs are more highly correlated with the observed annual cycle of TC numbers than uncoupled runs.

Most of the studies mentioned above have focused on the simulation of TC numbers over the annual cycle. However, few studies have investigated the accuracy of models in simulating the south–north movement of TC genesis locations and the effects of meridional migration of the WNPSH on this movement. In this study, we employed GCMs from CMIP6 HighResMIP to examine the simulations of the annual TC cycle over the WNP. We focused on the climatology of TC numbers and locations and the effects on TC location from large-scale environmental factors including the WNPSH. We also discussed the future changes in the annual cycle of TC activity. The remainder of this paper is organized as follows. In section 2, we briefly describe the observed data, model description, and methods of analysis. Section 3 shows the simulations of TC genesis activity and the analysis of genesis potential indices (GPIs) over the annual cycle. Section 4 discusses the possible causes of simulated bias. Section 5 shows the future projection of the TC annual cycle modulated by the changes in large-scale circulation. Discussion and conclusions are given in sections 6 and 7, respectively.

2. Data, models, and methods

a. Data

The observed data for seasonal cycles over 1979–2008 were compared against model simulations on dynamic and thermodynamic characteristics. Data on atmospheric conditions were obtained from the National Centers for Environmental Prediction (NCEP)–Climate Forecast System Reanalysis (CFSR) database with a $0.5° \times 0.5°$ longitude–latitude resolution (Saha et al. 2010). Version 1 of the Met Office Hadley Centre Sea Ice and Sea Surface Temperature dataset (HadISST1), which has a $1° \times 1°$ longitude–latitude resolution, was used to obtain sea surface temperature (Rayner et al. 2003). The precipitation data at a resolution of $2.5° \times 2.5°$ were obtained from satellite and gauge measurements performed by the Global Precipitation Climatology Project (GPCP), version 2.3 (Adler et al. 2018).

The observed TC data in the WNP were obtained from the Joint Typhoon Warning Center (JTWC). We only considered TCs with maximum wind speeds ≥ 35 kt (1 kt ≈ 0.51 m s^{-1}) (approximately 17.5 m s^{-1}). We defined the TC genesis location as the position of the first data point recorded in the lifetime of a TC.

b. Model simulations

We used six models from the European Union Horizon 2020 project PRIMAVERA (https://www.climateurope.eu/primavera/) under the CMIP6 HighResMIP experimental protocol (Haarsma et al. 2016). Each model runs at a lower and a higher horizontal resolution. We focused on the analysis of simulation with a higher resolution ranging from 50 to 25 km. These models are CMCC-CM2-VHR4 (Scoccimarro et al. 2017), CNRM-CM6-1-HR (Voldoire 2019), EC-Earth3P-HR (EC-Earth 2018), ECMWF-IFS-HR (Roberts et al. 2017), HadGEM3-GC31-HM (Roberts 2017), and MPI-ESM1-2-XR (von Storch et al. 2017), as described in Table 1. Each GCM completed the atmospheric (highresSST-present; tier 1) and coupled (hist-1950; tier 2) runs during 1950–2014. The future projections (tier 3) under the Shared Socioeconomic Pathways 5-8.5 (SSP5-8.5) scenario are also used to examine the future change in the annual cycle of TC activity. The CMIP6 HighResMIP protocol and the simulation design of these six model groups are detailed in Haarsma et al. (2016) and Roberts et al. (2020a), respectively.

TC locations and tracks from model simulations were obtained using the objective feature-tracking algorithm "TRACK" (Bengtsson et al. 2007; Strachan et al. 2013; Hodges et al. 2017). This algorithm used data on 6-h relative vorticity to track TCs on a common T63 spectral grid with warm-core criteria. The relative vorticities were first vertically averaged at the levels 850, 700, and 600 hPa on the analysis grid, and further tracking occurred if they exceeded 5×10^{-6} s^{-1} at each time step on a T63 grid. Only tracks that last at least 2 days were retained for further analysis. The tracking

TABLE 1. Concise list of PRIMAVERA (HighResMIP) model configurations.

Model name	Institution	Atmospheric nominal resolution (km)	Atmospheric model levels	Ocean resolution (°)
CMCC-CM2-VHR4	Fondazione Centro Euro-Mediterraneo sui Cambiamenti Climatici (CMCC)	25	26	0.25
CNRM-CM6-1-HR	Centre Europeen de Recherche et de Formation Avancee en Calcul Scientifique (CERFACS)	50	91	0.25
EC-Earth3P-HR	Royal Netherlands Meteorological Institute (KNMI); Swedish Meteorological and Hydrological Institute (SMHI); Barcelona Supercomputing Center (BSC); Consiglio Nazionale delle Ricerche (CNR)	50	91	0.25
ECMWF-IFS-HR	European Centre for Medium-Range Weather Forecasts (ECMWF)	25	91	0.25
HadGEM3-GC31-HM	Met Office Hadley Centre (MOHC)	50	85	0.08
MPI-ESM1-2-XR	Max Planck Institute for Meteorology (MPI-M)	50	95	0.4

proceeded by identifying the following criteria (Roberts et al. 2020a):

1) The relative vorticity at 850 hPa is $\geq 6 \times 10^{-5}$ s^{-1};
2) The difference in vorticity between 850 and 250 hPa is $>6 \times 10^{-5}$ s^{-1} to provide evidence of a warm core;
3) The vorticity center must exist at each level including 850, 700, 600, 500, and 250 hPa;
4) Criteria 1–3 must be jointly attained for at least four consecutive time steps (1 day) and only apply over the oceans;
5) Tracks must start within 30°S–30°N.

More detecting criteria are described in Roberts et al. (2020a). Modeled TC data were accessed from the Centre for Environmental Data Analysis (Roberts et al. 2020a,b).

c. Methods of analysis

We applied a GPI based on the work of Murakami and Wang (2010) to explore the annual cycle of TC genesis in connection with large-scale environmental variations. The GPI is defined as

$$\mathrm{GPI} = |10^5 \eta|^{3/2}\left(\frac{\mathrm{RH}}{50}\right)^3\left(\frac{V_{\mathrm{pot}}}{70}\right)^3(1 + 0.1V_s)^{-2}\left(\frac{-\omega + 0.1}{0.1}\right), \quad (1)$$

where η is the absolute vorticity at 850 hPa (s^{-1}), RH is the relative humidity at 600 hPa (%), V_{pot} is the maximum TC potential intensity (m s^{-1}) based on the study by Bister and Emanuel (2002), V_s is the magnitude of the vertical wind shear (m s^{-1}) between 850 and 200 hPa, and ω is the vertical pressure velocity at 500 hPa (Pa s^{-1}).

To quantify the relative contributions of individual terms to total GPI difference, we followed Li et al. (2013) in considering the difference between the atmospheric general circulation model (AGCM) and CGCM values for each term but fixed the multiple of the remaining terms as the climatology in AGCM.

3. Ability of HighResMIP to simulate the TC annual cycle and activity

a. Variation in TC genesis frequency over the annual cycle

Figure 1 illustrates the annual cycles of TC numbers in the WNP. In the observed data, the TC number increases substantially after June, peaks in August, and decreases noticeably after September (Fig. 1a). All AGCMs and CGCMs realistically simulated the annual cycle of TC frequency except MPI-ESM1-2-XR (Figs. 1b–g). The underestimation of TC numbers in the MPI-ESM1-2-XR has been reported in earlier studies (Roberts et al. 2020a,b; Tang et al. 2022). A further analysis suggested that this underestimation was likely due to an underestimation in the variance of vorticity at 850 hPa over the WNP. Because a multimodel ensemble mean may reduce the bias and uncertainty inherent in individual runs, we use the ensemble mean in the following analysis. For convenience, the ensembles of atmospheric runs and air–sea coupled runs are referred to as Ens-AGCM and Ens-CGCM, respectively. The MPI-ESM1-2-XR estimates were excluded from the ensemble mean due to their underestimation of TC numbers.

The annual cycle of TC frequency was successfully captured by the ensemble mean (Fig. 1a). Ens-AGCM and Ens-CGCM had temporal correlation coefficients larger than 0.9 in relation to the observed data. During the development stage of the WNP monsoon (June–September), the Ens-AGCM and the Ens-CGCM closely fit the observed TC numbers. However, the number of TCs decreased more gradually in the Ens-AGCM than in both the Ens-CGCM and observed data during the retreat stage of the WNP monsoon (after September).

Figure 2 depicts the spatial distribution of TC genesis frequency and midtropospheric geopotential height during the typhoon season. In June and July, most TCs formed in the Philippine Sea (Fig. 2a). In response to the annual cycle, the

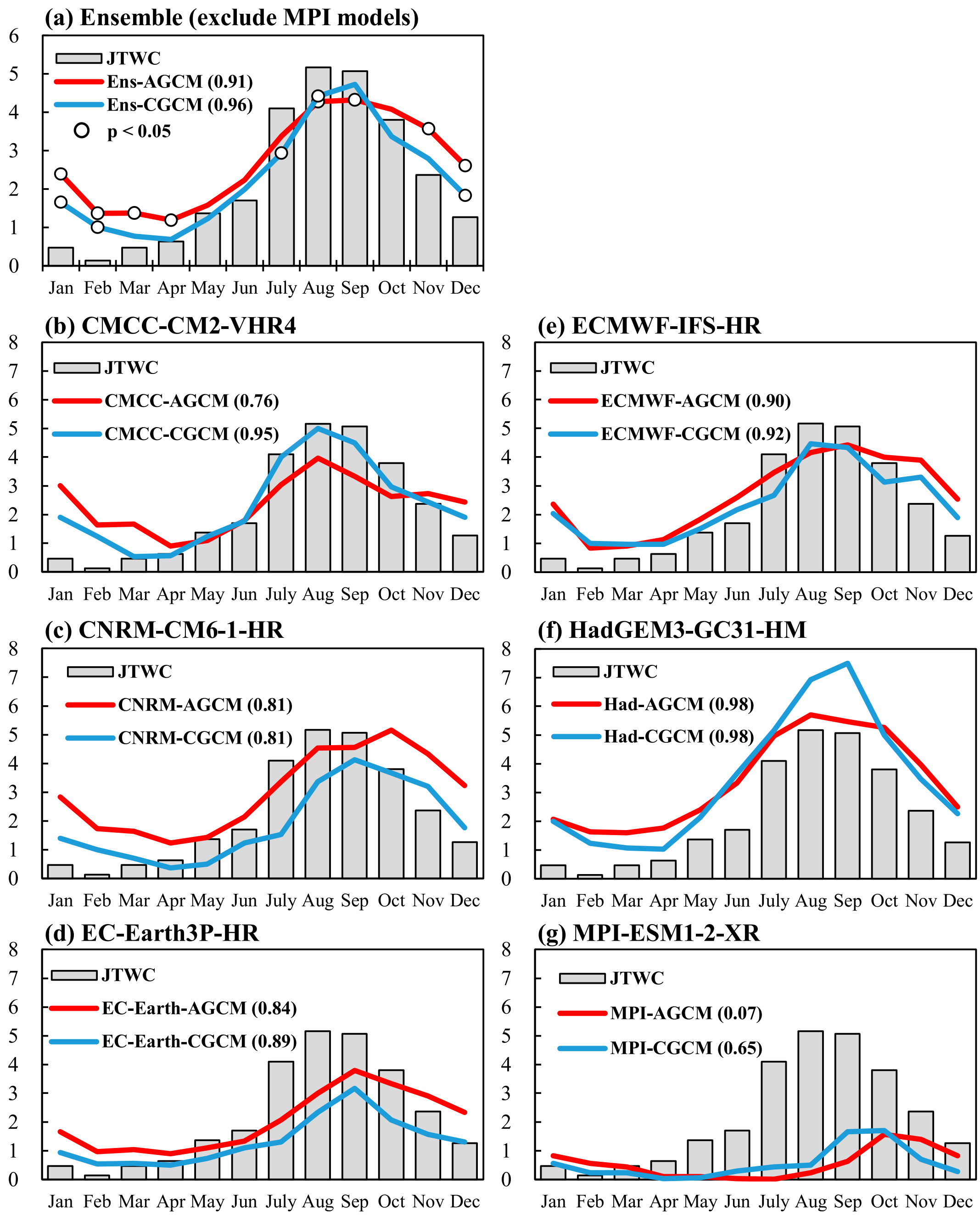

FIG. 1. Comparisons of the climatology (1979–2008) of the annual cycle of TC genesis numbers in the WNP between the observed data (gray bars), CMIP6 HighResMIP AGCM (red line), and CGCM (blue line) simulations from (a) the ensemble mean excluding MPI-ESM1-2-XR simulations (referred to as Ens-AGCM and Ens-CGCM) and (b)–(g) individual models. The numbers within parentheses indicate the temporal CC between simulation and observed data. The white circles in (a) indicate that the difference in the TC numbers between model simulation and observed data is statistically significant.

TC genesis locations extended eastward and migrated northward to the south of Japan during August–September (Fig. 2d). The locations migrated southward to the south of 20°N in October–November (Fig. 2g). The meridional migrations of TC genesis locations were primarily controlled by the location of the ridge of the WNPSH (WNP-SHR; see the dashed line in Fig. 2), which moved northward and southward in response to the period of monsoon development and retreat, respectively; that is, the TCs frequently formed south of the WNP-SHR (Figs. 2a,d,g). These results indicate that the

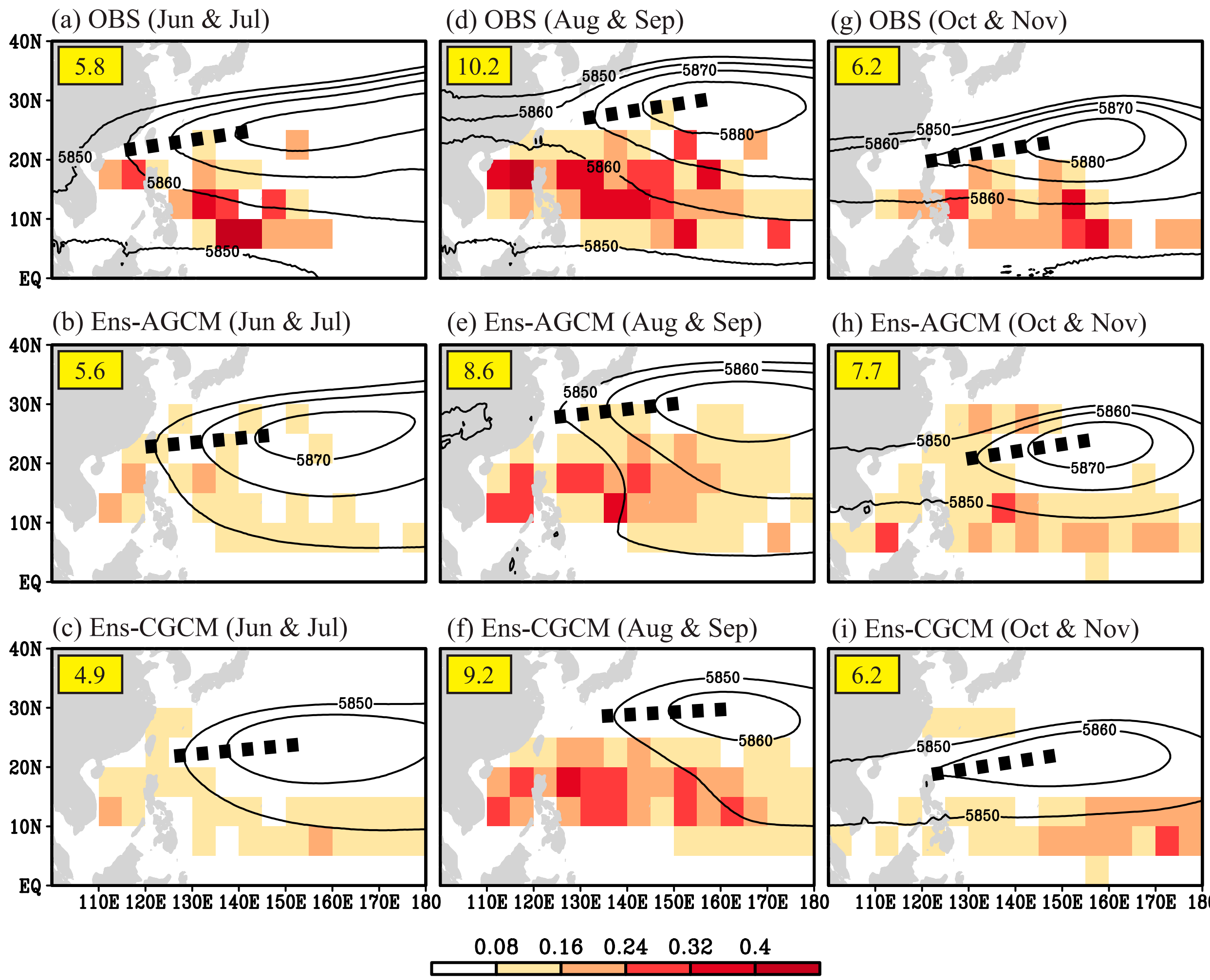

FIG. 2. Climatology of the TC formation frequency (numbers per year; shaded) and 500-hPa geopotential height (m; contour) with a ridge (black dotted line) during June–July for (a) observation, (b) Ens-AGCM, and (c) Ens-CGCM. (d)–(f) and (g)–(i) As in (a)–(c), but during August–September and October–November, respectively. The number in each picture indicates the TC count (per year) in the WNP.

location of the WNP-SHR plays a crucial role in determining the north extension of TC genesis locations.

Overall, both the Ens-AGCM and the Ens-CGCM reasonably simulated the meridional migration of the WNP-SHR and TC genesis locations in response to the annual cycle (Figs. 2b,c,e,f,h,i). For the June–July period, the Ens-AGCM simulated the TC genesis numbers and locations more accurately than the Ens-CGCM (Figs. 2b,c). The spatial correlation coefficient (CC) between the Ens-AGCM and the observed data (CC = 0.65) is higher than that between the Ens-CGCM and the observation (CC = 0.53). However, the Ens-AGCM has a lower skill in simulating the TC numbers after July than the Ens-CGCM. It underestimated (overestimated) the TC genesis numbers during August–September (October–November). The Ens-AGCM had a clear eastward shift in the WNP-SHR during October–November (cf. the dashed lines in Figs. 2h,g). This bias weakened the strength of the WNP-SHR in the Philippine Sea. TC genesis numbers were thus overestimated (underestimated) north (south) of 20°N in the Ens-AGCM (Fig. 2h). By contrast, the Ens-CGCM realistically captured the southward and westward retreat of the WNP-SHR (Fig. 2i). The simulation of the TC genesis location and the number was more accurate during the period of monsoon retreat.

b. GPI analysis

A GPI analysis was applied to investigate the effects of large-scale thermodynamic and dynamic factors on the discrepancy in TC genesis numbers and locations between the models and observed data. Figure 3 presents the climatologies of GPI and TC genesis frequency in the observed data and simulations for comparison. The observed GPIs closely fit the data for TC genesis, especially during August–September and October–November (Figs. 3d,g). Most TCs formed over the South China Sea and the Philippine Sea where high GPIs were observed. The meridional migration of larger GPIs realistically reproduced the meridional migration of TC genesis locations in response to the seasonal cycle (Figs. 3a,d,g).

Overall, the climatological GPIs and TC genesis locations shared a similar spatial pattern in both the Ens-AGCM and

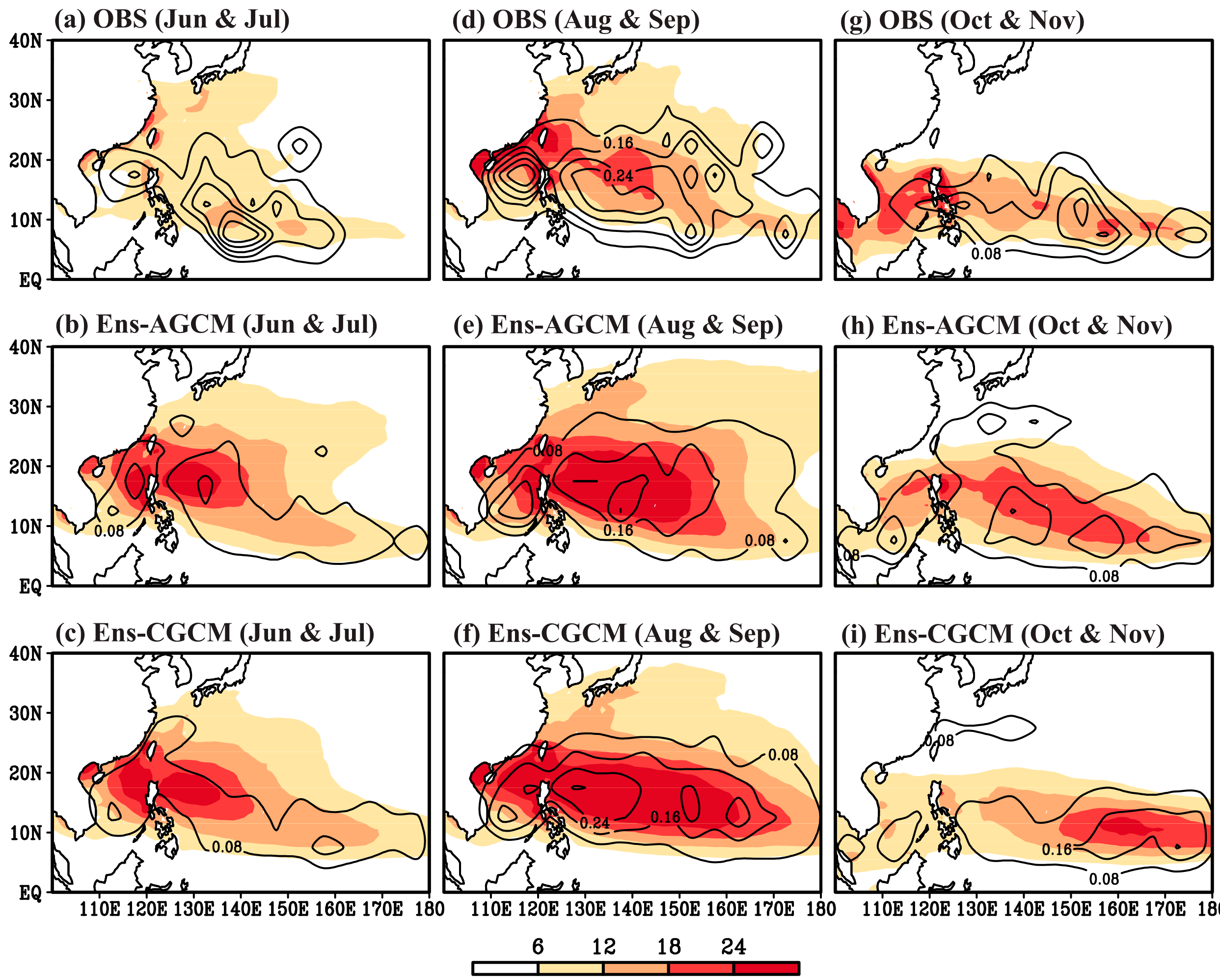

FIG. 3. GPI (shaded) and TC genesis (numbers per year; contour) distribution during June–July for (a) observation, (b) Ens-AGCM, and (c) Ens-CGCM. (d)–(f) and (g)–(i) As in (a)–(c), but during August–September and October–November, respectively.

Ens-CGCM during the entire typhoon season (Figs. 3b,c,e,f,h,i), although the magnitude of the GPIs was particularly overestimated during the development stage of the WNP monsoon (Figs. 3b,c,e,f). The meridional migration of the GPIs in response to the seasonal cycle also was reasonably simulated. These results indicate that GPIs are indeed useful indicators of the seasonal variation in the TC frequency in the WNP.

Because the Ens-AGCM was most inaccurate in simulating the annual cycle of TC activity (number and location) during August–September and October–November, we focused on these periods in our GPI analysis. Figure 4 illustrates the differences between the Ens-AGCM and the Ens-CGCM (Ens-AGCM minus Ens-CGCM) in total GPI and TC genesis frequency and the relative contribution of individual terms to the total GPI difference. In August and September, the distributions of GPI and TC genesis frequency differed similarly and exhibited a south–north tripole pattern (Fig. 4a). This tripole pattern approximately had a belt of negative GPI between 10° and 20°N and belts of opposite values south of 10°N and north of 20°N. The negative GPI substantially led to a greater underestimation of the TC genesis number compared with the Ens-CGCM. The GPI includes five terms, and the relative contribution of each term to the total GPI difference was estimated per the method of Li et al. (2013). Our estimate revealed that midtropospheric relative humidity and low-level cyclonic vorticity primarily contributed to the GPI difference (Fig. 4b).

In October and November, the distributions of GPI and TC genesis frequency also had a similar pattern and exhibited an east–west dipole structure (Fig. 4c); that is, the Ens-AGCM overestimated (underestimated) the GPI west (east) of 150°E compared with the Ens-CGCM. This overestimation of GPIs over the Philippine Sea resulted in a more gradual decrease in the TC genesis number compared with the Ens-CGCM during the monsoon retreat (Fig. 1a). An analysis of each term revealed that midtropospheric relative humidity dominated the GPI difference and that upward motion played a secondary role (Fig. 4d). The contributions of lower-level vorticity, maximum potential intensity, and vertical wind shear were not significant. Midtropospheric relative humidity, vertical motion, and the eastward shift of the WNP-SHR (Figs. 2h,i) worked in conjunction to create favorable conditions for TC genesis.

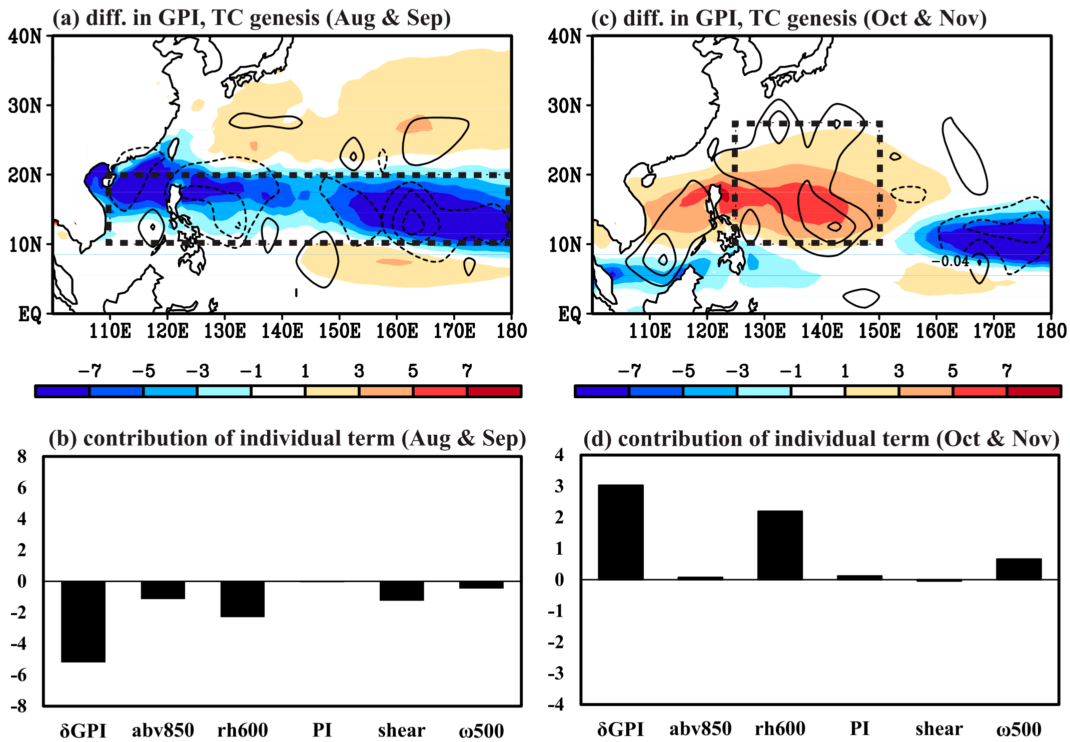

FIG. 4. The difference between the Ens-AGCM and Ens-CGCM simulations (Ens-AGCM minus Ens-CGCM) during August–September in (a) the GPI (shaded) and TC genesis frequency (numbers per year; contour), and (b) the relative contribution of individual terms of GPI over the domain where the change in the TC frequency was evident [black box in (a)]. (c),(d) As in (a),(b), but during October–November.

This accounts for the less rapid decrease in TC activity during October–November. Consequently, the underestimation of GPI in August–September and the overestimation of GPI in October–November resulted in a relatively flat seasonal cycle in the Ens-AGCM compared with the Ens-CGCM (Fig. 1a).

4. Possible causes for simulation bias in the Ens-AGCM

As indicated in Fig. 2, TC genesis numbers were underestimated (overestimated) during August–September (October–November) in the Ens-AGCM. This explains the bias of the Ens-AGCM in simulating the annual cycle of TC frequency. The possible causes for this bias are discussed in the following sections.

a. Atmospheric circulation in response to La Niña–like SST

Figure 5 presents the differences in the SST and the 850-hPa streamfunction between the Ens-AGCM and the Ens-CGCM (Ens-AGCM minus Ens-CGCM) for August–September and October–November. The SST difference has a La Niña–like pattern that persists through the summer to the autumn. Because the Ens-AGCM was forced by the observed SST as the lower boundary condition, the La Niña–like SST reflects an El Niño–like SST bias in the coupled models, a common feature seen in CMIP6 simulations (Zhang et al. 2023). Previous studies reported that the atmospheric response in the WNP to the ENSO-related SST anomalies (SSTAs) was seasonal dependent (Wang et al. 2000; Wang and Zhang 2002; Stuecker et al. 2015; Wu et al. 2017a). This is especially evident in monsoon regions like the WNP, where the basic flow (i.e., prevailing wind) is nearly opposite between the dry and wet monsoon seasons. The SSTA–mean flow interaction modified the atmospheric response to the same SSTAs. Consequently, the ENSO-related SSTAs tend to drive a large-scale cyclonic circulation anomaly over the WNP during the El Niño-developing summer. Conversely, an anticyclonic circulation anomaly was established in the WNP during the following autumn and winter (Wang et al. 2000; Wang and Zhang 2002; Stuecker et al. 2015; Wu et al. 2017a). It is widely accepted that this season-dependent circulation transition is related to a tight link between the phase of El Niño and the changes in the background mean state over the annual cycle (Wang et al. 2000; Wang and Zhang 2002; Wu et al. 2017b).

The similar results were identified in this study except for the atmospheric response to La Niña–like SSTAs. A Gill-type large-scale anticyclonic circulation anomaly, in response to the La Niña–like SST, was identified in the subtropical Pacific in the Northern Hemisphere during August–September (Fig. 5a). This anticyclonic anomaly weakened the WNP monsoon trough, which in turn suppressed TC genesis. These unfavorable conditions contributed to the Ens-AGCM's underestimation of TC numbers in summer compared with the estimates given by the Ens-CGCM (Figs. 2e,f). The anticyclonic anomaly

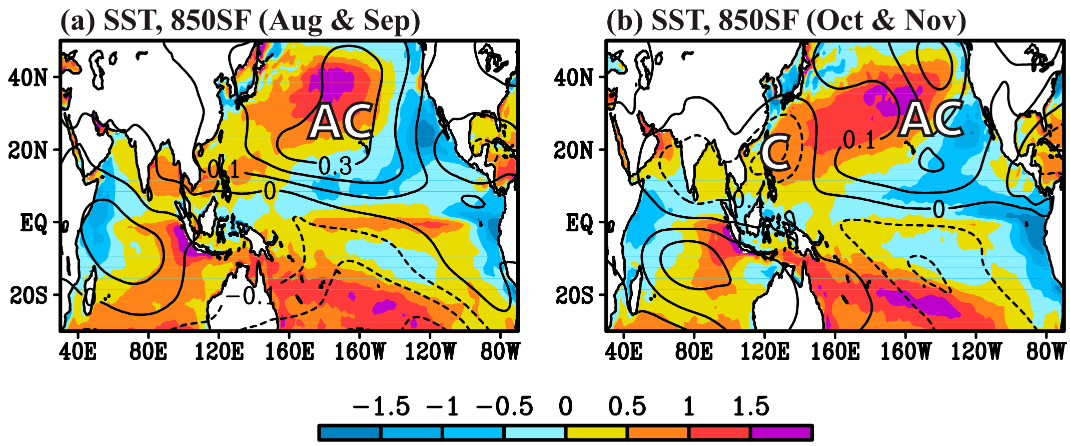

FIG. 5. The difference in the SST (°C; shaded) and 850-hPa streamfunction (10^7 m^2 s^{-1}; contour) between the Ens-AGCM and Ens-CGCM simulations (Ens-AGCM minus Ens-CGCM) during (a) August–September and (b) October–November. The characters AC and C in the panel represent the locations of anomalous anticyclone and cyclone, respectively.

in the WNP persisted for the entire monsoon season, with the center shifting east in autumn (Fig. 5b). Additionally, a cyclonic anomaly moved eastward from the Indian Ocean to the Philippine Sea during October–November. The cyclonic anomaly provided favorable large-scale conditions for TC genesis. Consequently, the decrease in TC numbers during October–November estimated by the Ens-AGCM was more gradual than the decrease seen in both the observed data and Ens-CGCM.

b. Season-dependent local air–sea interaction

Wang et al. (2000) uncovered the mechanism of local air–sea interaction to explain the establishment and maintenance of anticyclonic anomalies in the Philippine Sea during the mature phase of El Niño. In this study, the atmospheric response in the Philippine Sea during October–November reflected the working of this mechanism. During August–September, the anticyclonic anomaly in the Philippine Sea was part of a large-scale anticyclonic anomaly in response to La Niña–like SST (Figs. 5a and 6a). During October–November, this Gill-type anticyclonic anomaly moved eastward, and the Philippine Sea was covered by a cyclonic anomaly that moved from the Indian Ocean. The southwesterly associated with this cyclonic anomaly was against the northeasterly prevailing wind in the central-western tropical Pacific (Figs. 5b and 6b). The cyclonic anomaly weakened the northeasterly trade wind, which warmed the SST in the Philippine Sea and cooled the SST along the coast of East China through wind–evaporation–SST (WES) feedback (Wang et al. 2000). This feedback favored an east–west-distributed SST anomaly, extending along the East China coast and the Philippine Sea. The east–west SST anomaly itself probably created a circulation anomaly that maintained the cyclonic anomaly in the Philippine Sea. In sum, the eastward shift in large-scale anticyclonic anomaly

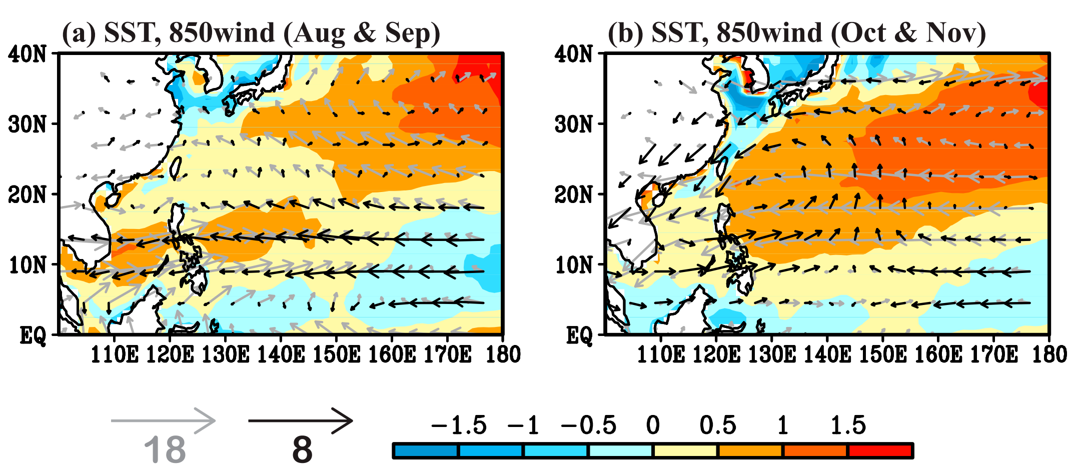

FIG. 6. Climatology of 850-hPa wind (m s^{-1}; gray vector) in Ens-CGCM and the difference in the SST (°C; shaded) and 850-hPa wind (m s^{-1}; black vector) between the Ens-AGCM and Ens-CGCM simulations (Ens-AGCM minus Ens-CGCM) during (a) August–September and (b) October–November.

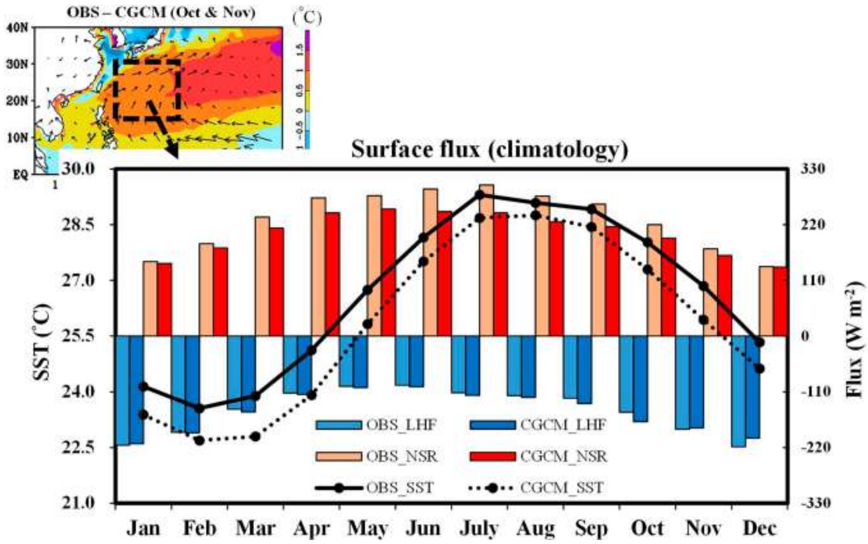

FIG. 7. A comparison of time series for the averaged climatological SST (black curves), latent heat flux (bars in red tone), and net downward shortwave radiation (bars in blue tone) between observation and Ens-CGCM over the region where WES feedback was evident (dashed box in the upper-left panel). The upper-left panel indicates the differences in SST (°C; shaded) and 850-hPa winds (m s^{-1}; vector) between observation and Ens-CGCM (observation minus Ens-CGCM) during October–November.

in response to the annual cycle led to the establishment of a cyclonic anomaly in the WNP through local wind–evaporation–SST feedback when the prevailing wind shifted to northeasterly.

Figure 7 shows the comparison of the annual cycle of SST and surface flux averaged in the regions where WES feedback occurred between the Ens-CGCM and observed data. The Ens-CGCM realistically captured the annual cycle of individual fluxes, although the incoming shortwave radiations were underestimated. This underestimation is likely due to the negative SST–cloud–radiation (SCR) feedback (Ramanathan and Collins 1991; Li et al. 2000), which results from the cyclonic anomaly in response to El Niño-like SST bias during the typhoon season. The latent heat flux exchange cools the SST, and its effect increases from summer to winter in response to the establishment of a prevailing northeasterly wind (Wang et al. 2000). During October–November, the magnitude of latent heat is close to that of the incoming shortwave radiation, and the SST in this region rapidly decreased. The overestimation of latent heat and the underestimation of net downward shortwave radiation in Ens-CGCM contributed to an SST cold bias in the Philippine Sea.

The same analysis was applied to the Ens-AGCM. It revealed that the incoming shortwave radiation, as identified in Ens-CGCM, was also underestimated (not shown). This bias was due to the prescribed SST and a lack of negative SST–cloud–radiation feedback in the AGCMs. A tropical warm SST usually plays an active role and can force a lower-level cyclonic circulation and convection anomaly (Figs. 5b and 6b). The overestimation of convection substantially decreased the incoming shortwave radiation. The prescribed warm SST also led to an overestimation of latent heat flux throughout almost the entire year. Finally, this cyclone anomaly and warmer SST provide more favorable large-scale conditions for TC genesis, leading to an overestimation of TC genesis numbers in October and November.

Mean TC genesis locations were strongly influenced by the WNP-SHR, which migrated northward to Japan in summer and returned to the South China Sea in autumn. The southward migration of the WNP-SHR in autumn suppressed TC genesis and caused TCs to only occur south of 20°N. The lack of air–sea interaction in the Ens-AGCM, combined with the seasonal cycle, probably caused the models to underestimate the WNP-SHR. This underestimation gave rise to an overestimation of the GPI and TC numbers in the Philippine Sea (Fig. 4). Consequently, the annual cycle of TC numbers in the Ens-AGCM did not exhibit the same rapid decrease seen in both the observed data and Ens-CGCM.

5. Future changes in TC annual cycle and possible causes for the changes

Changes in the annual cycle of TC activity in future projection under global warming and possible causes for the changes were investigated in this section. Figure 8 compares the annual cycle of TC genesis counts between the present climate (1979–2008) and a mid-21st-century (2021–50) simulation under the high-emission SSP5-8.5 scenario (O'Neill et al. 2016). Overall, the annual mean of the TC genesis number decreased by approximately 5% in Ens-AGCM and 7% in Ens-CGCM during 2021–50, respectively. This declining trend in the WNP aligns with the findings from previous studies employing high-resolution models (Knutson et al. 2020). Additionally, Ens-AGCM simulated a faster drop in the TC genesis number in the

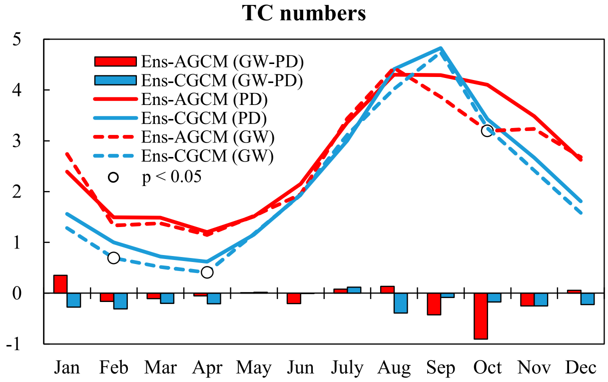

FIG. 8. Comparisons of the annual cycle of TC genesis numbers between present-day (PD; 1979–2008) and global warming (GW; 2021–50) simulations using ensemble means. Data from ECMWF-IFS-HR were excluded due to the lack of future simulations. The solid (dotted) lines indicate the PD (GW) simulation. The bars indicate the difference between PD and GW simulations (GW minus PD). The white circles indicate that the difference in TC numbers between PD and GW simulations is statistically significant.

future than that in the present climate during autumn, particularly in the monsoon retreat period (October–November). By contrast, the TC annual cycle in Ens-CGCM revealed minor changes in the future.

Figure 9 presents the future changes in the spatial distribution of TC genesis frequency and 850-hPa winds in August–September and October–November. For the Ens-AGCM, the reduction primarily occurred over the main TC genesis region and was possibly caused by the low-level anticyclonic anomalous flows in the WNP (Figs. 9a,c). Notably, the change in the TC genesis frequency in August–September seems to exhibit an east–west dipole structure (Fig. 9a); that is, the increase (decrease) in the TC frequency occurred west (east) of 150°E. This concentration of the increased TC frequency was likely attributed to the weakened eastward propagation of intraseasonal oscillations modified by the enhancement of WNPSH (Tam and Lau 2005; Hong and Li 2009). By contrast, the main change in Ens-CGCM was that the TC genesis location shifts northward during the monsoon retread period (Fig. 9d), a phenomenon also noted in previous studies (Sharmila and Walsh 2018; Shan and Yu 2020; Feng et al. 2021).

The distinct response of the annual cycle of the TC genesis frequency in the future between the Ens-AGCM and the Ens-CGCM was likely attributed to the different changes in large-scale circulation (Fig. 10). For the Ens-AGCM, SSTs exhibited a greater warming in the northern Indian Ocean (NIO) and WNP and a smaller warming in the central-eastern North Pacific (Fig. 10a). This led a zonal SST gradient over the Indo-

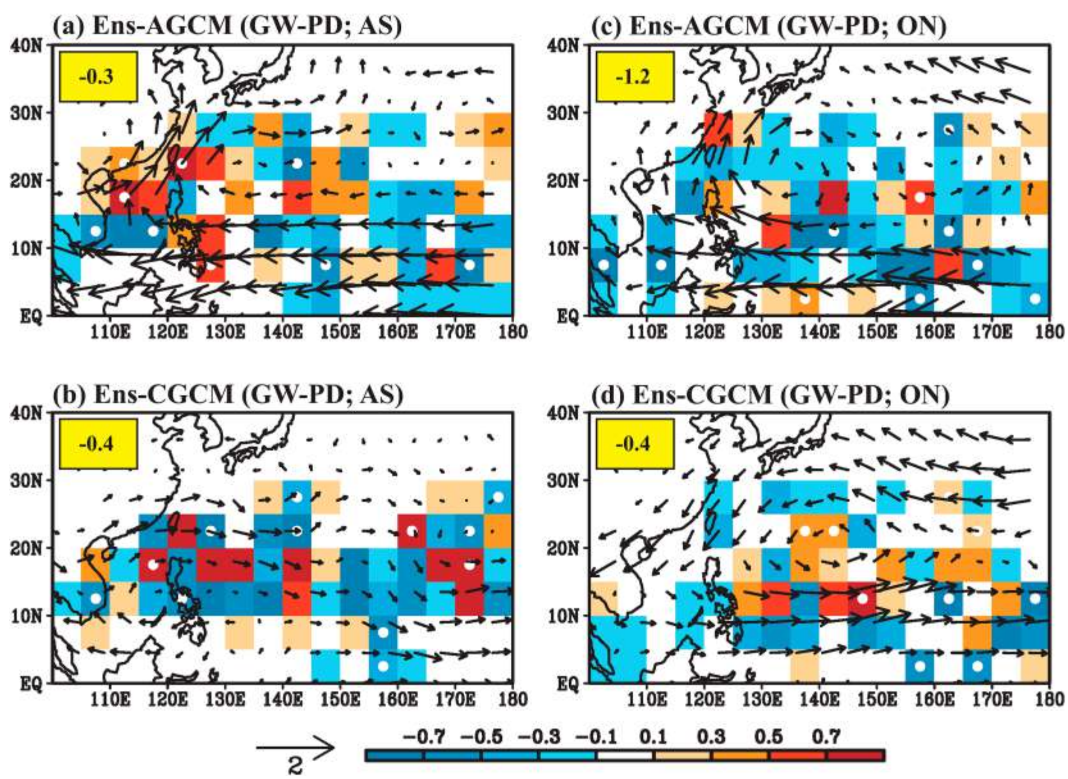

FIG. 9. (a) Difference in the TC genesis frequency (numbers per 10 years; shaded) and 850-hPa wind (m s^{-1}; vector) between PD and GW simulations (GW minus PD) in Ens-AGCM during August–September. (b) As in (a), but for Ens-CGCM. (c),(d) As in (a),(b), but during October–November. The number in each panel indicates the total difference in the TC count (per year) over the WNP. The stippling in each panel indicates that the difference in the TC genesis frequency is statistically significant at the 90% confidence level.

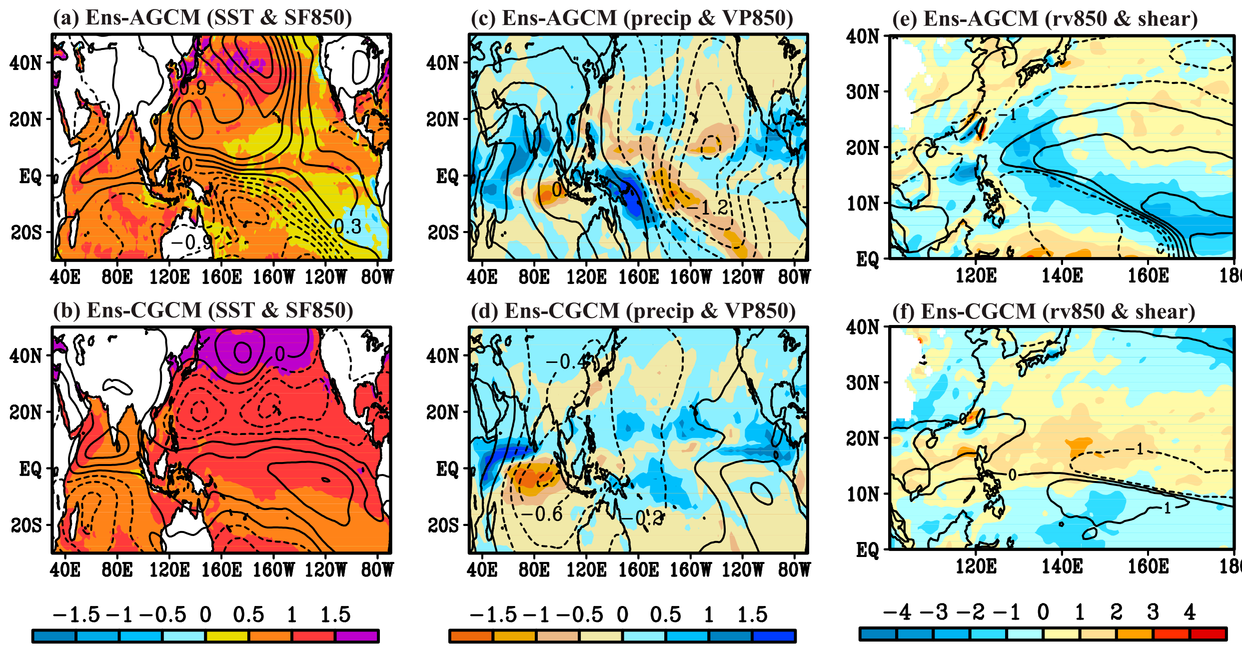

FIG. 10. (a) Difference in the SST (°C; shaded) and 850-hPa streamfunction (10^6 m^2 s^{-1}; contour) between PD and GW simulations (GW minus PD) in Ens-AGCM during October–November. (b) As in (a), but for Ens-CGCM. (c),(d) As in (a),(b), but for the precipitation (mm day^{-1}; shaded) and 850-hPa velocity potential (10^6 m^2 s^{-1}; contour). (e),(f) As in (a),(b), but for the 850-hPa relative vorticity (10^{-6} s^{-1}; shaded) and vertical wind shear defined as the difference of horizontal wind speed between 850 and 200 hPa (m s^{-1}; contour) over the WNP.

Pacific, which provided a favorable boundary condition for the enhancement of the WNP subtropical high (Fig. 10a). Meanwhile, a positive (negative) precipitation anomaly over the NIO (WNP) was identified (Fig. 10c). The precipitation anomalies created a Walker circulation anomaly in the Indo-Pacific, characterized by upward (downward) motions over the NIO (WNP). The enhanced-WNPSH-associated negative relative vorticity and positive vertical wind shear, as well as subsidence anomalies, suppressed TC formation in the WNP (Fig. 10e). Conversely, Ens-CGCM projected warmer SSTs over the whole tropical North Pacific in the future (Fig. 10b). The causes for a warmer SST projection in Ens-CGCM are complex and beyond the scope of this paper. Some studies reported that changes in the representation of aerosol schemes or differences in the prescribed concentrations of greenhouse gases between CMIP5 and CMIP6 models are likely contributors (Zelinka et al. 2020; Wyser et al. 2020a,b). A cyclonic circulation anomaly accompanied with upward motion anomalies and positive precipitation anomalies was identified north of 10°N (Figs. 10b,d). This cyclonic anomaly provided a favorable environment for TC formation. It modulated the vorticity and vertical wind shear, favoring a northward shift in the mean TC genesis location in a warming climate (Figs. 9d and 10f).

6. Discussion

This study indicates that the HighResMIP simulations reasonably capture the annual cycle of TC activity in the WNP. However, the Ens-AGCM tends to overestimate the atmospheric response to prescribed SST (Lau and Ploshay 2009); that is, a positive SST anomaly is expected to cause above-normal precipitation (Fig. 11). However, the SST–precipitation relationship is usually negatively correlated in the WNP during the boreal summer monsoon (Wang et al. 2005). An anticyclonic anomaly with below-normal rainfall may cause a positive SST anomaly through associated large-scale subsidence. However, deep convection is usually accompanied by a negative SST anomaly due to cloud–radiation–SST feedback (Ramanathan and Collins 1991; Li et al. 2000; Hong et al. 2008). These processes were not successfully captured in the AGCMs, causing significant bias in the Ens-AGCM in simulating the annual cycle of TC activity.

Song and Zhou (2014) reported that CGCMs from CMIP5 improved substantially the simulation of summertime WNPSH compared with that in AGCMs. A consistent result was found in the HighResMIP of CMIP6 (Figs. 2 and 6). The cold SST bias in the WNP has a compensation effect on improving the simulation of the annual cycle of WNP-SHR and the TC activity compared with AGCMs.

Since only an ensemble of five models might be doubtful, we expanded the ensemble size to seven, incorporating ECMWF-IFS-LR and MPI-ESM1-2-XR models with 50-km resolution. This extension aims to examine the sensitivity of the discrepancies in the TC annual cycle between AGCMs and CGCMs. The estimate revealed that the number of TCs also increased (decreased) more gradually during August–September (October–November) in the ensemble of seven AGCMs than in the ensemble of seven CGCMs (Fig. 12).

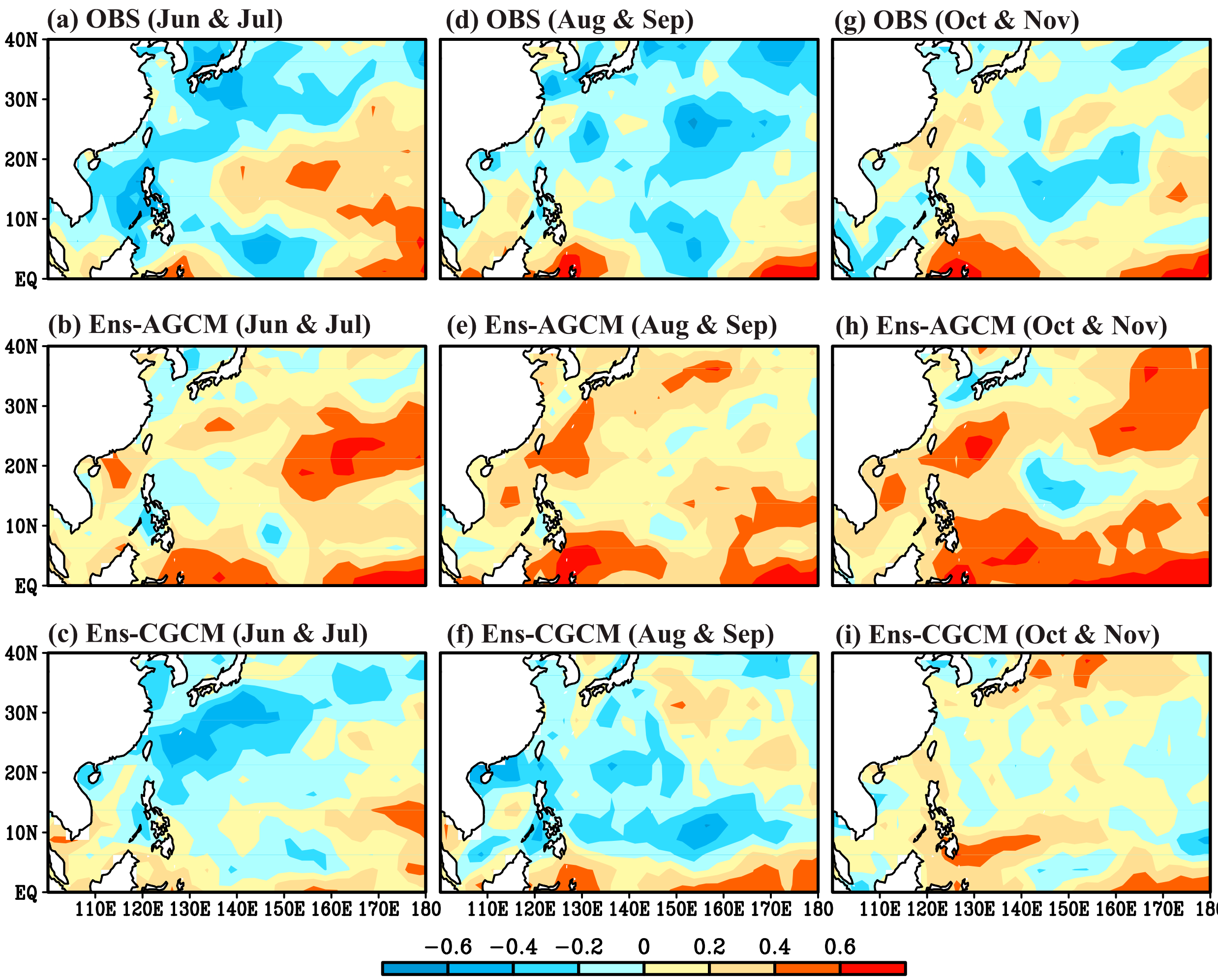

FIG. 11. The point CCs between SST and precipitation during June–July for (a) observation, (b) Ens-AGCM, and (c) Ens-CGCM. (d)–(f) and (g)–(i) As in (a)–(c), but for August–September and October–November, respectively.

This robustness of the results increases our confidence in our analysis.

In addition to the TC genesis frequency, the annual cycle of intense TCs (≧category 3) was investigated. In observation, the intense TCs similar to the total TCs exhibit an evident annual cycle with a peak in autumn (Fig. 13). Most of AGCMs and CGCMs realistically simulated the annual cycle of intense TCs but with underestimation, especially for the Ens-CGCM, in autumn. Additionally, the observed seasonal advance, reported in a recent study (Shan et al. 2023), was not captured by all GCMs (not shown). These results suggest that high-resolution models still face challenges in accurately capturing intense TC numbers and trends. For future changes, both Ens-AGCM and Ens-CGCM projected a similar annual cycle compared to their present climates, but Ens-AGCM showed a noticeable decrease during summer and fall, particularly in October (Fig. 14). Note that underestimating the TC intensity may lead to uncertainty in projecting intense TCs in a warming climate. Thus, the limitation of TC intensity simulation should be considered when investigating future changes in severe TCs by using HighResMIP models.

7. Conclusions

This study evaluated the performance of HighResMIP models in simulating TC activity over its annual cycle, including the number and location of TCs, in the WNP. Potential changes in the annual cycle of TC activity under global warming were also investigated. The possible causes of biases in simulating TC activity were addressed. The results are summarized as follows (Fig. 15).

1) The Ens-AGCM and the Ens-CGCM reasonably simulated the annual cycle of TC numbers. However, TC numbers were underestimated (overestimated) during the monsoon development (retreat) in the Ens-AGCM compared with the observed data and with the Ens-CGCM. This bias caused the Ens-AGCM to fail to simulate a rapid decrease in the TC number after September.

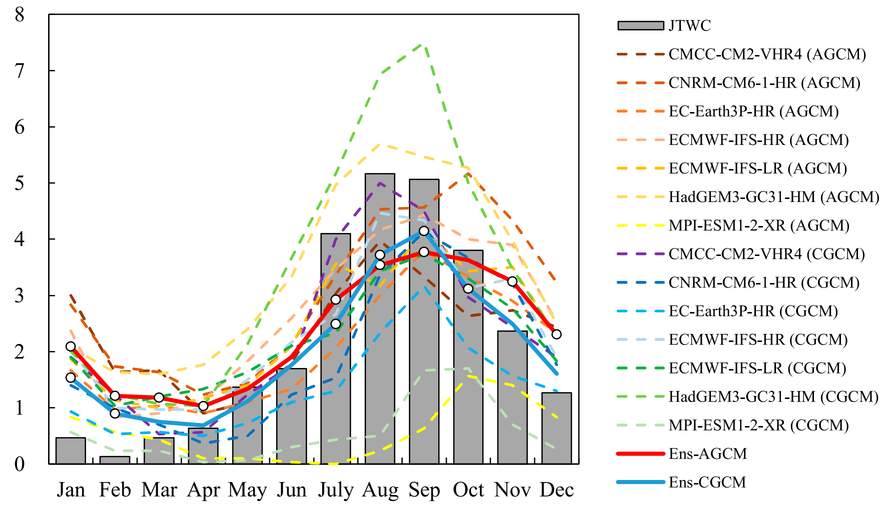

FIG. 12. As in Fig. 1, but for the addition of ECMWF-IFS-LR simulations.

2) The Ens-AGCM and the Ens-CGCM both captured the meridional migration of the WNP-SHR in response to the seasonal cycle. Nevertheless, the WNP-SHR in the Ens-AGCM exhibited a west (east) shift bias during August–September (October–November). This bias may result in an underestimation (overestimation) of TC numbers for August–September (October–November). The mean locations of TC genesis also shifted substantially northward in October–November due to the eastward shift of the WNP-SHR.
3) The GPI analysis revealed that the overestimations of GPI and TC numbers over the South China Sea and the Philippine Sea (10°–20°N, 110°–150°E) during October–November in the Ens-AGCM were due to overestimations of midtropospheric relative humidity and upward motion. The underestimations of the GPI between 10° and 20°N during August–September were due to underestimations of midtropospheric relative humidity and low-tropospheric vorticity.
4) The differences in simulations of the annual cycle of TC numbers between runs using coupled and uncoupled models can be explained by a large-scale circulation anomaly over the WNP in response to a La Niña–like SST difference between the Ens-AGCM and the Ens-CGCM (Fig. 15). The Gill-type anticyclonic anomaly in response to the La Niña–like SST dominated large-scale circulation in the WNP during August–September. The anticyclonic anomaly shifted eastward during October–November. During this period, a cyclonic anomaly occurred in the Philippine Sea and was maintained through local air–sea interaction, a WES positive feedback mechanism (Wang et al. 2000). This cyclonic anomaly favored TC activity and probably caused an overestimation of TC numbers in the Philippine Sea.
5) AGCMs and CGCMs exhibiting a similarity revealed that the annual mean of the TC number will decrease by approximately 5%–7% in future climate (2021–50). Ens-AGCM projected a faster drop in the annual cycle during the monsoon retreat period. By contrast, Ens-CGCM simulated minor changes in the annual cycle but with a northward shift in the TC genesis location during the monsoon retreat period.
6) A faster drop in Ens-AGCM was attributed to compound factors. The enhanced WNPSH, accompanied with downward motion anomalies, modulated the low-tropospheric vorticity and vertical wind shear and may lead to a more rapid decrease in the TC numbers. Conversely, a cyclonic circulation anomaly projected by Ens-CGCM, accompanied with upward motion anomalies, was identified off-equator and favored TC genesis location shifting northward in the future.

Our comparison between the atmospheric and coupled runs of the CMIP6 HighResMIP highlights the importance of the air–sea interaction in capturing the meridional migration of the WNP-SHR over the annual cycle. Realistic simulation of the WNP-SHR is crucial to the accuracy of a model in simulating the annual cycle of TC activity in the WNP. These results help us better predict seasonal TCs and understand the complex interactions among SST, atmospheric circulation, and TC genesis over the annual cycle.

This meridional migration of TC formation indirectly influences the landfall frequency of TCs over East Asia (Harr and Elsberry 1991; Kim et al. 2005). An important finding in this study shows that while the high-resolution Atmospheric Model Intercomparison Project (AMIP) simulation has sufficient ability to capture the annual mean of TC genesis numbers (Dwyer et al. 2015; Tsou et al. 2016; Tang et al. 2022), it exhibits lower skill in simulating the annual cycle of TC numbers and genesis locations compared to the coupled model (CGCM). In addition to the WNP region, we also investigated the annual cycle of TC activity in the eastern North Pacific and North Atlantic. Overall, the results yield consistency and indicate that Ens-CGCM can realistically capture the annual cycle of TC numbers with better skill than Ens-AGCM, although Ens-CGCM underestimates TC numbers during the peak season (August–October) in the North Atlantic (not

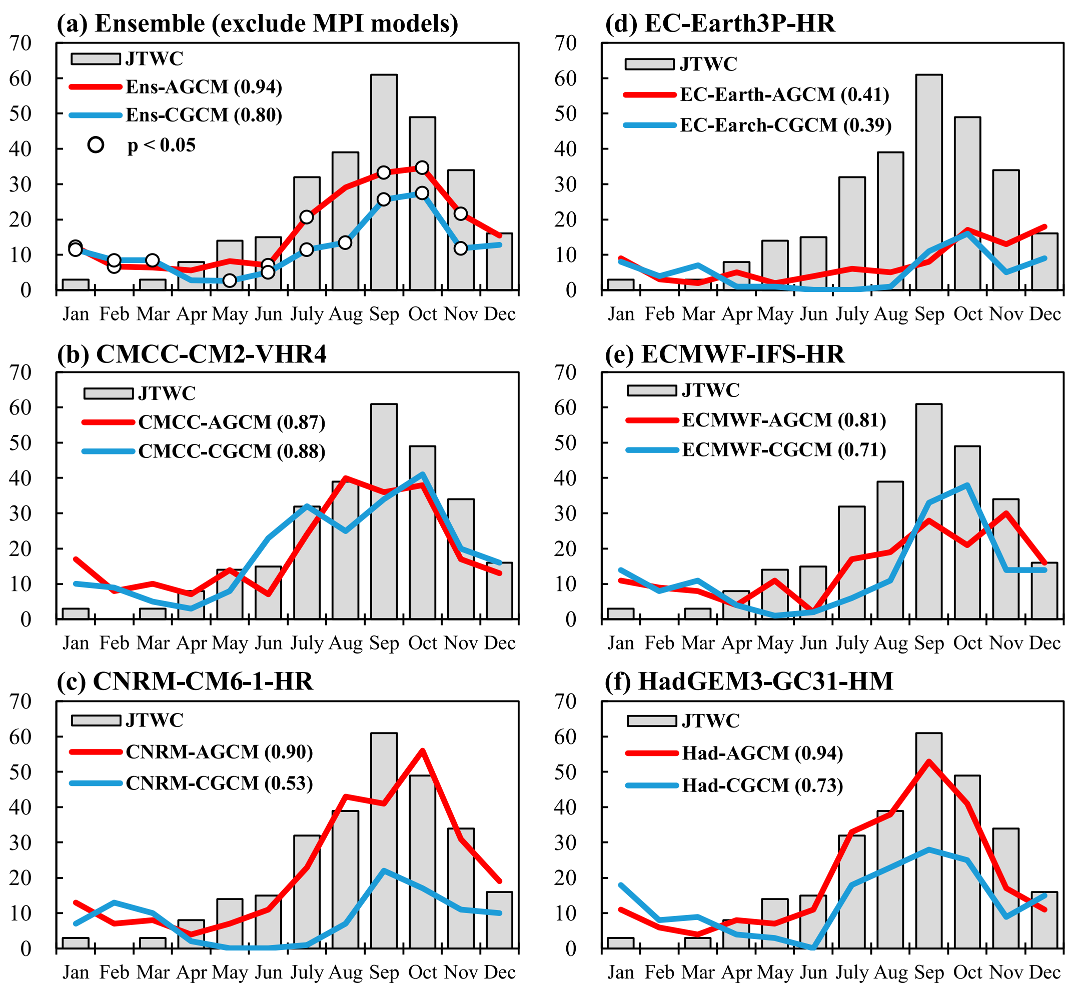

FIG. 13. Annual cycle of the number of intense TCs (number per 30 years) for the observed data (gray bars), AGCM (red line), and CGCM (blue line) in (a) ensemble means excluding MPI-ESM1-2-XR simulations, and (b)–(f) individual models. The numbers within parentheses indicate the temporal CC between simulation and observation. The white circles in (a) indicate that the difference in TC numbers between simulation and observation is statistically significant.

shown). The ability of Ens-CGCM to simulate the TC's annual cycle encourages us to investigate TC landfalls in different seasons in both the present climate and future projections. This work will be presented in the other papers.

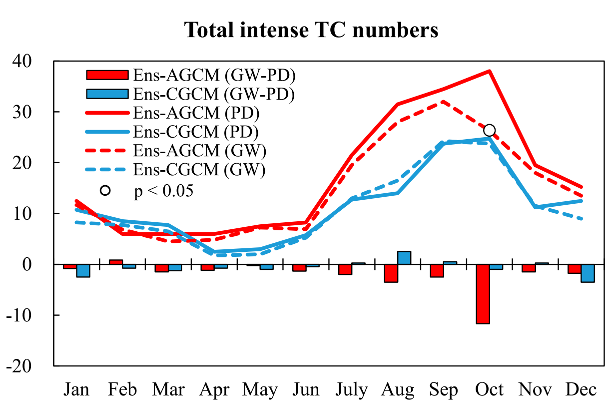

FIG. 14. As in Fig. 8, but for the number of intense TCs.

Acknowledgments. The analysis described in this paper was supported by the National Science and Technology Council (NSTC), Taiwan, under Grants 112-2811-M-845-001, 112-2811-M-845-002, and 111-2111-M-845-001. We are grateful to Professor Tim Li for his valuable comments. We also wish to express our gratitude to Mr. HC Liang for his assistance in downloading the model outputs used. This manuscript was edited by Wallace Academic Editing.

Data availability statement. The observed monthly atmospheric conditions and sea surface temperature were obtained from the National Centers for Environmental Prediction (NCEP)–Climate Forecast System Reanalysis (CFSR; https://rda.ucar.edu/datasets/ds093.2/) and the Met Office Hadley Centre Sea Ice and Sea Surface Temperature dataset, version 1 (HadISST1; https://www.metoffice.gov.uk/hadobs/hadisst/data/download.html), respectively. The observed tropical cyclone data in the western North Pacific were obtained from the Joint Typhoon Warning Center (JTWC; https://www.metoc.navy.

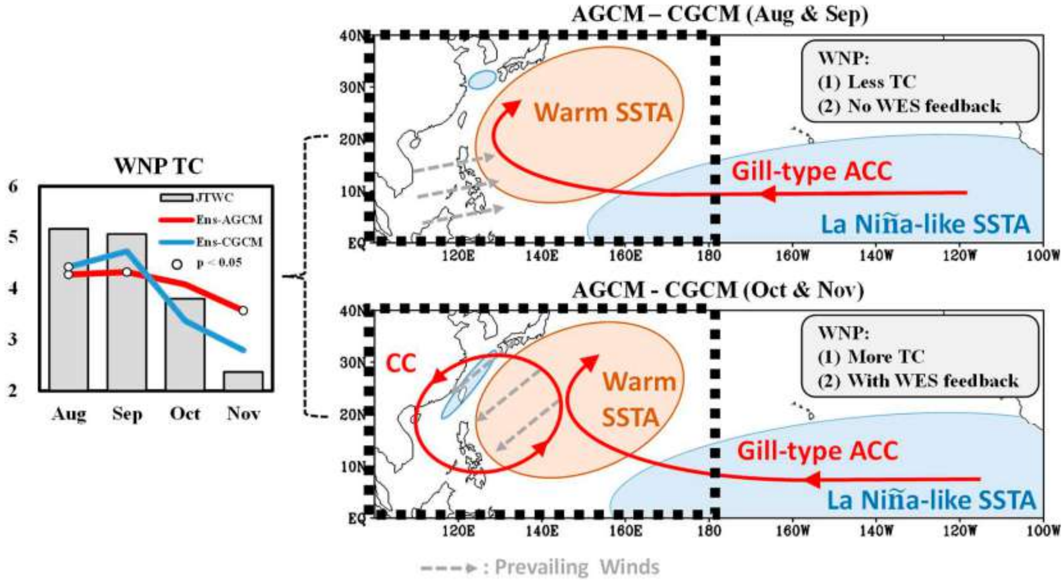

FIG. 15. Schematic diagram illustrates the causes of bias for the TC genesis frequency simulated by Ens-AGCM in the WNP (black dotted boxes) during the monsoon development and retreat periods by comparing the Ens-AGCM and Ens-CGCM.

mil/jtwc/jtwc.html?western-pacific). The model outputs from CMIP6 HighResMIP were obtained from the Earth System Grid Federation nodes (https://esgf-node.llnl.gov/projects/cmip6/). The tropical cyclone tracks detected by the TRACK algorithm were obtained from the Centre for Environmental Data Analysis (https://data.ceda.ac.uk/badc/highresmip-derived/data/storm_tracks/TRACK).

REFERENCES

Adler, R. F., and Coauthors, 2018: The Global Precipitation Climatology Project (GPCP) monthly analysis (new version 2.3) and a review of 2017 global precipitation. *Atmosphere*, **9**, 138, https://doi.org/10.3390/atmos9040138.

Bengtsson, L., K. I. Hodges, and M. Esch, 2007: Tropical cyclones in a T159 resolution global climate model: Comparison with observations and re-analyses. *Tellus*, **59A**, 396–416, https://doi.org/10.1111/j.1600-0870.2007.00236.x.

Bister, M., and K. A. Emanuel, 2002: Low frequency variability of tropical cyclone potential intensity 1. Interannual to interdecadal variability. *J. Geophys. Res.*, **107**, 4801, https://doi.org/10.1029/2001JD000776.

Camargo, S. J., 2013: Global and regional aspects of tropical cyclone activity in the CMIP5 models. *J. Climate*, **26**, 9880–9902, https://doi.org/10.1175/JCLI-D-12-00549.1.

Chen, J.-M., P.-H. Tan, L. Wu, J.-S. Liu, and H.-S. Chen, 2017: Climatological analysis of passage-type tropical cyclones from the western North Pacific into the South China Sea. *Terr. Atmos. Ocean. Sci.*, **28**, 327–343, https://doi.org/10.3319/TAO.2016.10.04.02.

Chen, K.-C., C.-H. Tsou, C.-C. Hong, H.-H. Hsu, and C.-Y. Tu, 2023: Effect of model resolution on simulation of tropical cyclone landfall in East Asia based on a comparison of 25- and 50-km HiRAMs. *Climate Dyn.*, **61**, 2085–2101, https://doi.org/10.1007/s00382-023-06668-z.

Chia, H. H., and C. F. Ropelewski, 2002: The interannual variability in the genesis location of tropical cyclones in the northwest Pacific. *J. Climate*, **15**, 2934–2944, https://doi.org/10.1175/1520-0442(2002)015<2934:TIVITG>2.0.CO;2.

Dwyer, J. G., S. J. Camargo, A. H. Sobel, M. Biasutti, K. A. Emanuel, G. A. Vecchi, M. Zhao, and M. K. Tippett, 2015: Projected twenty-first-century changes in the length of the tropical cyclone season. *J. Climate*, **28**, 6181–6192, https://doi.org/10.1175/JCLI-D-14-00686.1.

EC-Earth, 2018: EC-Earth-Consortium EC-Earth3P-HR model output prepared for CMIP6 HighResMIP. Earth System Grid Federation, accessed 23 August 2021, https://doi.org/10.22033/ESGF/CMIP6.2323.

Feng, X., N. P. Klingaman, and K. I. Hodges, 2021: Poleward migration of western North Pacific tropical cyclones related to changes in cyclone seasonality. *Nat. Commun.*, **12**, 6210, https://doi.org/10.1038/s41467-021-26369-7.

Gilford, D. M., S. Solomon, and K. A. Emanuel, 2017: On the seasonal cycles of tropical cyclone potential intensity. *J. Climate*, **30**, 6085–6096, https://doi.org/10.1175/JCLI-D-16-0827.1.

Haarsma, R. J., and Coauthors, 2016: High Resolution Model Intercomparison Project (HighResMIP v1.0) for CMIP6. *Geosci. Model Dev.*, **9**, 4185–4208, https://doi.org/10.5194/gmd-9-4185-2016.

Harr, P. A., and R. L. Elsberry, 1991: Tropical cyclone track characteristics as a function of large-scale circulation anomalies. *Mon. Wea. Rev.*, **119**, 1448–1468, https://doi.org/10.1175/1520-0493(1991)119<1448:TCTCAA>2.0.CO;2.

Hodges, K., A. Cobb, and P. L. Vidale, 2017: How well are tropical cyclones represented in reanalysis datasets? *J. Climate*, **30**, 5243–5264, https://doi.org/10.1175/JCLI-D-16-0557.1.

Hong, C.-C., and T. Li, 2009: The extreme cold anomaly over southeast Asia in February 2008: Roles of ISO and ENSO. *J. Climate*, **22**, 3786–3801, https://doi.org/10.1175/2009JCLI2864.1.

——, ——, LinHo, and J.-S. Kug, 2008: Asymmetry of the Indian Ocean dipole. Part I: Observational analysis. *J. Climate*, **21**, 4834–4848, https://doi.org/10.1175/2008JCLI2222.1.

Kim, J.-H., C.-H. Ho, and C.-H. Sui, 2005: Circulation features associated with the record-breaking typhoon landfall on Japan in 2004. *Geophys. Res. Lett.*, **32**, L14713, https://doi.org/10.1029/2005GL022494.

Knutson, T., and Coauthors, 2020: Tropical cyclones and climate change assessment: Part II: Projected response to anthropogenic warming. *Bull. Amer. Meteor. Soc.*, **101**, E303–E322, https://doi.org/10.1175/BAMS-D-18-0194.1.

Lander, M. A., 1994: An exploratory analysis of the relationship between tropical storm formation in the western North Pacific and ENSO. *Mon. Wea. Rev.*, **122**, 636–651, https://doi.org/10.1175/1520-0493(1994)122<0636:AEAOTR>2.0.CO;2.

Lau, N.-C., and J. J. Ploshay, 2009: Simulation of synoptic- and subsynoptic-scale phenomena associated with the East Asian summer monsoon using a high-resolution GCM. *Mon. Wea. Rev.*, **137**, 137–160, https://doi.org/10.1175/2008MWR2511.1.

Li, T., T. F. Hogan, and C.-P. Chang, 2000: Dynamic and thermodynamic regulation of ocean warming. *J. Atmos. Sci.*, **57**, 3353–3365, https://doi.org/10.1175/1520-0469(2000)057<3353:DATROO>2.0.CO;2.

Li, Z., W. Yu, T. Li, V. S. N. Murty, and F. Tangang, 2013: Bimodal character of cyclone climatology in the Bay of Bengal modulated by monsoon seasonal cycle. *J. Climate*, **26**, 1033–1046, https://doi.org/10.1175/JCLI-D-11-00627.1.

——, H.-L. Ren, M. Lu, and F. Zhou, 2024: Interannual variations of westward extension area of western Pacific subtropical high and its relationship with precipitation in East Asia. *Atmos. Res.*, **298**, 107148, https://doi.org/10.1016/j.atmosres.2023.107148.

Liu, K. S., and J. C. L. Chan, 2013: Inactive period of western North Pacific tropical cyclone activity in 1998–2011. *J. Climate*, **26**, 2614–2630, https://doi.org/10.1175/JCLI-D-12-00053.1.

Manganello, J. V., and Coauthors, 2012: Tropical cyclone climatology in a 10-km global atmospheric GCM: Toward weather-resolving climate modeling. *J. Climate*, **25**, 3867–3893, https://doi.org/10.1175/JCLI-D-11-00346.1.

Murakami, H., and B. Wang, 2010: Future change of North Atlantic tropical cyclone tracks: Projection by a 20-km-mesh global atmospheric model. *J. Climate*, **23**, 2699–2721, https://doi.org/10.1175/2010JCLI3338.1.

O'Neill, B. C., and Coauthors, 2016: The Scenario Model Intercomparison Project (ScenarioMIP) for CMIP6. *Geosci. Model Dev.*, **9**, 3461–3482, https://doi.org/10.5194/gmd-9-3461-2016.

Ramanathan, V., and W. Collins, 1991: Thermodynamic regulation of ocean warming by cirrus clouds deduced from observations of the 1987 El Niño. *Nature*, **351**, 27–32, https://doi.org/10.1038/351027a0.

Rayner, N. A., D. E. Parker, E. B. Horton, C. K. Folland, L. V. Alexander, D. P. Rowell, E. C. Kent, and A. Kaplan, 2003: Global analyses of sea surface temperature, sea ice, and night marine air temperature since the late nineteenth century. *J. Geophys. Res.*, **108**, 4407, https://doi.org/10.1029/2002JD002670.

Ritchie, E. A., and G. J. Holland, 1999: Large-scale patterns associated with tropical cyclogenesis in the western Pacific. *Mon. Wea. Rev.*, **127**, 2027–2043, https://doi.org/10.1175/1520-0493(1999)127<2027:LSPAWT>2.0.CO;2.

Roberts, C. D., R. Senan, F. Molteni, S. Boussetta, and S. Keeley, 2017: ECMWF ECMWF-IFS-HR model output prepared for CMIP6 HighResMIP. Earth System Grid Federation, accessed 23 August 2021, https://doi.org/10.22033/ESGF/CMIP6.2461.

Roberts, M., 2017: MOHC HadGEM3-GC31-HM model output prepared for CMIP6 HighResMIP. Earth System Grid Federation, accessed 23 August 2021, https://doi.org/10.22033/ESGF/CMIP6.446.

Roberts, M. J., and Coauthors, 2015: Tropical cyclones in the UPSCALE ensemble of high-resolution global climate models. *J. Climate*, **28**, 574–596, https://doi.org/10.1175/JCLI-D-14-00131.1.

——, and Coauthors, 2020a: Impact of model resolution on tropical cyclone simulation using the HighResMIP–PRIMAVERA multimodel ensemble. *J. Climate*, **33**, 2557–2583, https://doi.org/10.1175/JCLI-D-19-0639.1.

——, and Coauthors, 2020b: Projected future changes in tropical cyclones using the CMIP6 HighResMIP multimodel ensemble. *Geophys. Res. Lett.*, **47**, e2020GL088662, https://doi.org/10.1029/2020GL088662.

Saha, S., and Coauthors, 2010: The NCEP Climate Forecast System Reanalysis. *Bull. Amer. Meteor. Soc.*, **91**, 1015–1058, https://doi.org/10.1175/2010BAMS3001.1.

Scoccimarro, E., A. Bellucci, and D. Peano, 2017: CMCC CMCC-CM2-VHR4 model output prepared for CMIP6 HighResMIP. Earth System Grid Federation, accessed 23 August 2021, https://doi.org/10.22033/ESGF/CMIP6.1367.

Shan, K., and X. Yu, 2020: Enhanced understanding of poleward migration of tropical cyclone genesis. *Environ. Res. Lett.*, **15**, 104062, https://doi.org/10.1088/1748-9326/abaf85.

——, Y. Lin, P.-S. Chu, X. Yu, and F. Song, 2023: Seasonal advance of intense tropical cyclones in a warming climate. *Nature*, **623**, 83–89, https://doi.org/10.1038/s41586-023-06544-0.

Sharmila, S., and K. J. E. Walsh, 2018: Recent poleward shift of tropical cyclone formation linked to Hadley cell expansion. *Nat. Climate Change*, **8**, 730–736, https://doi.org/10.1038/s41558-018-0227-5.

——, ——, M. Thatcher, S. Wales, and S. Utembe, 2020: Real world and tropical cyclone world. Part I: High-resolution climate model verification. *J. Climate*, **33**, 1455–1472, https://doi.org/10.1175/JCLI-D-19-0078.1.

Sobel, A. H., A. A. Wing, S. J. Camargo, C. M. Patricola, G. A. Vecchi, C. Y. Lee, and M. K. Tippett, 2021: Tropical cyclone frequency. *Earth's Future*, **9**, e2021EF002275, https://doi.org/10.1029/2021EF002275.

Song, F., and T. Zhou, 2014: The climatology and interannual variability of East Asian summer monsoon in CMIP5 coupled models: Does air–sea coupling improve the simulations? *J. Climate*, **27**, 8761–8777, https://doi.org/10.1175/JCLI-D-14-00396.1.

Strachan, J., P. L. Vidale, K. Hodges, M. Roberts, and M.-E. Demory, 2013: Investigating global tropical cyclone activity with a hierarchy of AGCMs: The role of model resolution. *J. Climate*, **26**, 133–152, https://doi.org/10.1175/JCLI-D-12-00012.1.

Stuecker, M. F., F.-F. Jin, A. Timmermann, and S. McGregor, 2015: Combination mode dynamics of the anomalous northwest Pacific anticyclone. *J. Climate*, **28**, 1093–1111, https://doi.org/10.1175/JCLI-D-14-00225.1.

Tam, C.-Y., and N.-C. Lau, 2005: The Impact of ENSO on atmospheric intraseasonal variability as inferred from observations and GCM simulations. *J. Climate*, **18**, 1902–1924, https://doi.org/10.1175/JCLI3399.1.

Tang, Y., J. Huangfu, R. Huang, and W. Chen, 2022: Simulation and projection of tropical cyclone activities over the western

North Pacific by CMIP6 HighResMIP. *J. Climate*, **35**, 7771–7794, https://doi.org/10.1175/JCLI-D-21-0760.1.

Tsou, C.-H., P.-Y. Huang, C.-Y. Tu, C.-T. Chen, T.-P. Tzeng, and C.-T. Cheng, 2016: Present simulation and future typhoon activity projection over western North Pacific and Taiwan/East coast of China in 20-km HiRAM climate model. *Terr. Atmos. Ocean. Sci.*, **27**, 687–703, https://doi.org/10.3319/TAO.2016.06.13.04.

Voldoire, A., 2019: CNRM-CERFACS CNRM-CM6-1-HR model output prepared for CMIP6 HighResMIP. Earth System Grid Federation, accessed 23 August 2021, https://doi.org/10.22033/ESGF/CMIP6.1387.

von Storch, J.-S., and Coauthors, 2017: MPI-M MPI-ESM1.2-XR model output prepared for CMIP6 HighResMIP. Earth System Grid Federation, accessed 23 August 2021, https://doi.org/10.22033/ESGF/CMIP6.10290.

Wang, B., and J. C. L. Chan, 2002: How strong ENSO events affect tropical storm activity over the western North Pacific. *J. Climate*, **15**, 1643–1658, https://doi.org/10.1175/1520-0442(2002)015<1643:HSEEAT>2.0.CO;2.

——, and Q. Zhang, 2002: Pacific–East Asian teleconnection. Part II: How the Philippine Sea anomalous anticyclone is established during El Niño development. *J. Climate*, **15**, 3252–3265, https://doi.org/10.1175/1520-0442(2002)015<3252:PEATPI>2.0.CO;2.

——, R. Wu, and X. Fu, 2000: Pacific–East Asian teleconnection: How does ENSO affect East Asian climate? *J. Climate*, **13**, 1517–1536, https://doi.org/10.1175/1520-0442(2000)013<1517:PEATHD>2.0.CO;2.

——, Q. Ding, X. Fu, I.-S. Kang, K. Jin, J. Shukla, and F. Doblas-Reyes, 2005: Fundamental challenge in simulation and prediction of summer monsoon rainfall. *Geophys. Res. Lett.*, **32**, L15711, https://doi.org/10.1029/2005GL022734.

Wang, C., and B. Wang, 2019: Tropical cyclone predictability shaped by western Pacific subtropical high: Integration of trans-basin sea surface temperature effects. *Climate Dyn.*, **53**, 2697–2714, https://doi.org/10.1007/s00382-019-04651-1.

Wu, B., T. Zhou, and T. Li, 2017a: Atmospheric dynamic and thermodynamic processes driving the western North Pacific anomalous anticyclone during El Niño. Part I: Maintenance mechanisms. *J. Climate*, **30**, 9621–9635, https://doi.org/10.1175/JCLI-D-16-0489.1.

——, ——, and ——, 2017b: Atmospheric dynamic and thermodynamic processes driving the western North Pacific anomalous anticyclone during El Niño. Part II: Formation processes. *J. Climate*, **30**, 9637–9650, https://doi.org/10.1175/JCLI-D-16-0495.1.

Wyser, K., T. van Noije, S. Yang, J. von Hardenberg, D. O'Donnell, and R. Döscher, 2020a: On the increased climate sensitivity in the EC-Earth model from CMIP5 to CMIP6. *Geosci. Model Dev.*, **13**, 3465–3474, https://doi.org/10.5194/gmd-13-3465-2020.

——, E. Kjellstrom, T. Koenigk, H. Martins, and R. Doscher, 2020b: Warmer climate projections in EC-Earth3-Veg: The role of changes in the greenhouse gas concentrations from CMIP5 to CMIP6. *Environ. Res. Lett.*, **15**, 054020, https://doi.org/10.1088/1748-9326/ab81c2.

Yang, B., and Coauthors, 2019: Better monsoon precipitation in coupled climate models due to bias compensation. *npj Climate Atmos. Sci.*, **2**, 43, https://doi.org/10.1038/s41612-019-0100-x.

Zelinka, M. D., T. A. Myers, D. T. McCoy, S. Po-Chedley, P. M. Caldwell, P. Ceppi, S. A. Klein, and K. E. Taylor, 2020: Causes of higher climate sensitivity in CMIP6 models. *Geophys. Res. Lett.*, **47**, e2019GL085782, https://doi.org/10.1029/2019GL085782.

Zhang, Q., B. Liu, S. Li, and T. Zhou, 2023: Understanding models' global sea surface temperature bias in mean state: From CMIP5 to CMIP6. *Geophys. Res. Lett.*, **50**, e2022GL100888, https://doi.org/10.1029/2022GL100888.